A Numerical Investigation into the Injury Potential of Three-year-old Children Seated in Forward Facing Child Safety Seats During Side Impact Crashes in Far Side Configurations

Qian Wang, Tanya Kapoor, William Altenhof
University of Windsor
Department of Mechanical
Automotive and Materials Engineering

Andrew Howard
The Hospital for Sick Children
Division of Orthopedic Surgery

Abstract

This research focuses on the injury potential of children seated in forward facing child restraint seats during side impact crashes. Side dynamic sled tests were conducted by NHTSA using the existing FMVSS 213 seat fixture oriented at both 90° and 45° relative to the motion of the sled buck. A half sine pulse and a scaled FMVSS 213 pulse were used in the tests. All the tests were conducted at a test velocity of 32 km/h (20 mph) and a peak acceleration of 17 g's. A forward-facing Hybrid III 3-year-old child dummy positioned in a child restraint seat (CRS) with LATCH and the top tether in far side configurations were used in the tests. Details of the sled tests were stated in FMVSS 213 ANPRM. A finite element model of the child restraint seat was developed using FEMB for simulation in LS-DYNA. The child seat model, which included all CAD surfaces provided by Century/Graco Corporation, was fully deformable and was previously validated for frontal impacts. Three side impact simulations were completed for data comparison. (i) using the half sine acceleration pulse with the seat oriented at 90° relative to the motion of the sled, (ii) using the half sine acceleration pulse with the seat oriented at 45° relative to the motion of the sled, and (iii) using scaled FMVSS 213 acceleration pulse with the seat oriented at 90° relative to the motion of the sled. Validation of the numerical model was completed by comparing the head injury criteria (HIC) values and chest accelerations from the experimental and numerical tests. The simulation results were generally in good agreement to the experimental observations. Further studies were conducted to confine lateral movement of the dummy's head by adding energy absorbing foam blocks in the head region of the CRS. It was observed from the simulation results that foam padding was effective in reducing the injury potential of the child dummy.

1. Introduction

According to The National Highway Traffic Safety Administration (NHTSA) [1], motor vehicle crashes are the leading cause of death for children of age from 3 to 14 years old. For passenger vehicle child occupants, ages 0 to 8 years old, data from FARS for 1991–2000 showed that [2], regardless of whether the child was seated in the front seat or rear seat, frontal and side crashes accounted for most child occupant fatalities. Fifty-one percent of front seat child occupant fatalities were in frontal crashes, and 31 percent were in side impact crashes. For rear seat child occupants, frontal impacts and side impact crashes accounted for 44 percent and 42 percent of the fatalities respectively.

Seating position relative to the point of impact is a factor in side impact crash fatalities. Data from NHTSA demonstrated that 22 percent of the 3,018 front seat child fatalities were killed in near side impacts [3]. Of the 3,826 rear seat fatalities, 25 percent involved near side impacts. Of the 682 children ages 0 to 8 years old who were killed in side impacts and were secured in child

restraints, 64 percent (434) were seated in the near side position. The remaining 36 percent of the fatalities (248) for children in child restraints were seated either in the middle seating position or in the far side position.

In a side crash involving three vehicles, a two and 1/2 years old child occupant sustained severe cervical dislocation, brain stem injury, and left rib fracture, which are illustrated in Figure 1. These injuries were a result of multiple impacts occurred when a Pontiac Grand Prix (Figure 2), which the child was seated in, and a Honda Accord, followed by impact between the Grand Prix and Dodge Caravan. The child occupant was seated in the rear location of the vehicle in a forward facing child restraint with a top tether. Compared to the normal neck physiology presented, Figure 1 clearly shows the severe dislocation between the head base and the first cervical vertebrae.

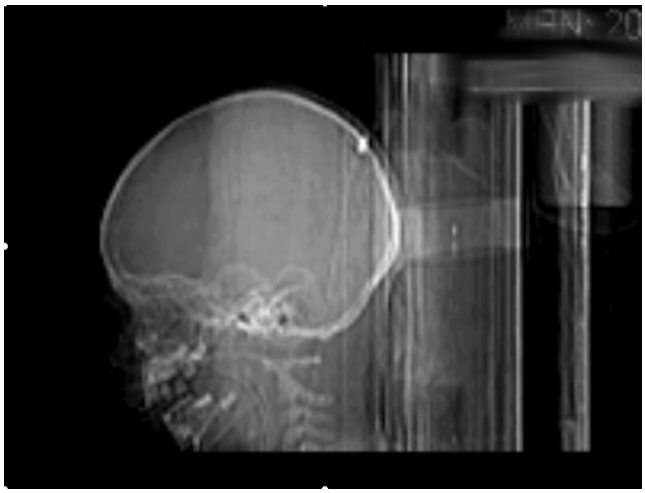

Figure 1. Child occupant injuries of side impact, Case 10 [4].

Figure 2. Pontiac Grand Prix, Case 10 [4].

2. Experimental Methods

Side impact dynamic sled tests were conducted by NHTSA using the existing FMVSS 213 seat fixture oriented at both 90° and 45° relative to the motion of the sled buck. A 1/2 sine pulse and a scaled FMVSS 213 pulse were used in the tests and are shown in Figure 3 and Figure 4. All the tests were conducted at a test velocity of 32 km/h (20 mph) and a peak acceleration of 17 G's. A forward-facing Hybrid III 3-year-old child dummy positioned in a child restraint seat with LATCH and the top tether in far side configuration was used in the tests. Injury data recorded during the side impact tests are shown in Table 1 and taken from reference [5].

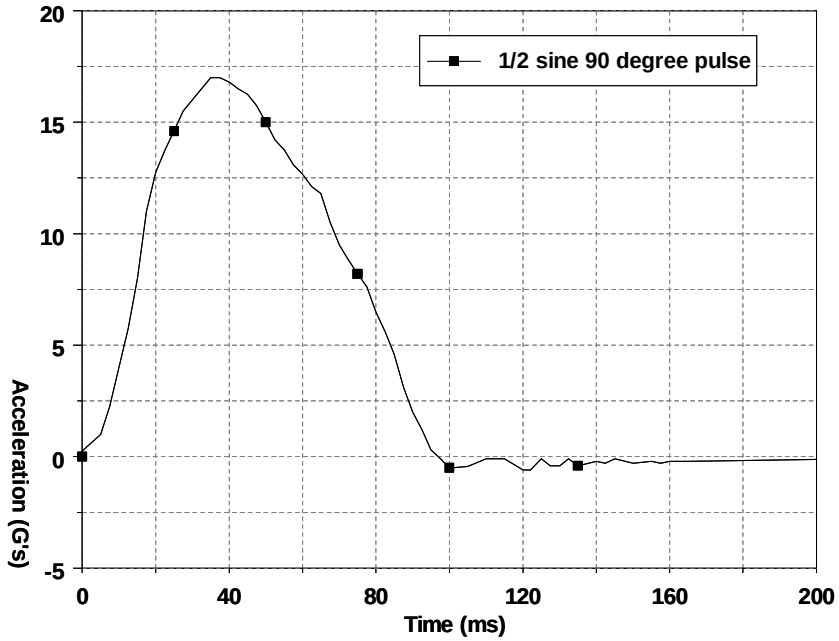

Figure 3. Half sine 90° pulse.

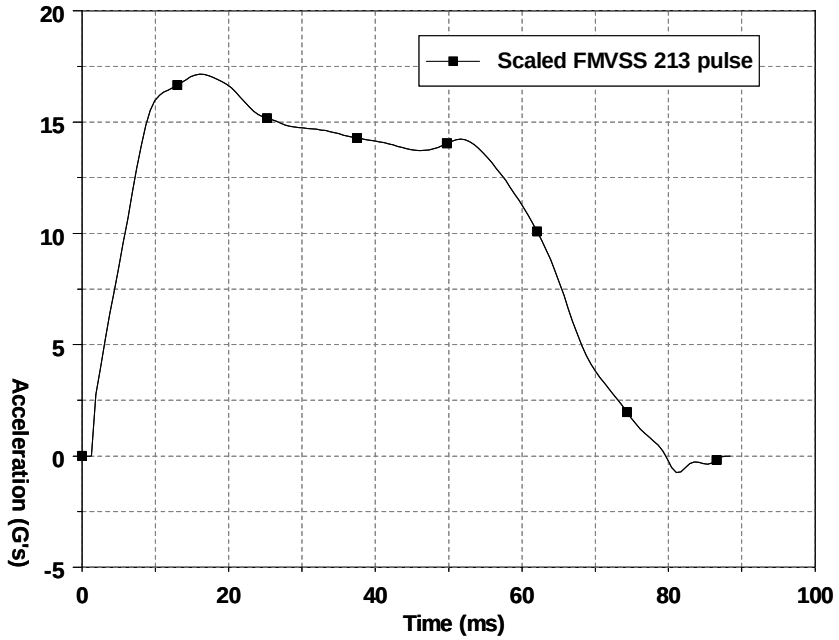

Figure 4. Scaled FMVSS 213 pulse.

Table 1. Summary of experimental testing observations for side impact at 45° and 90°[5].

Test No.	Test configuration	HIC_{15}	$HIC_{unlimited}$	Chest Accel. (G's)	Peak Ten.	Peak Com.
1	1/2 sine - 45°	122	226	29.1	963	318
2	1/2 sine - 45°	150	255	31.8	419	950
3	1/2 sine - 45° - no tether	122	268	26.4	493	436
4	1/2 sine - 45° - no tether	131	240	27.9	430	698
5	1/2 sine - 90°	76	160	23.8	253	670
6	1/2 sine - 90°	107	159	23.3	600	985
7	1/2 sine - 90° - no tether	99	200	23.8	113	643
8	1/2 sine - 90° - no tether	93	170	25.9	316	861
9	Scaled 213 - 90°	67	135	21.3	278	876
10	Scaled 213 - 90° - no tether	71	168	24.1	322	678

3. Numerical Methods

3.1 Modeling of the deformable child seat

The child safety seat, as well as all other components of the numerical model including the seat buck, the CRS webbing and the CRS foam pad, was meshed using FEMB. The child seat was modeled using Computer Aided Design (CAD) surfaces provided by Century/Graco Corp. Tensile testing was completed on specimens extracted from various portions of the CRS to determine mechanical characteristics of the CRS polypropylene material. Changes in the thickness of panel sections from the CRS were investigated and measured with a Vernier caliper. It was observed that the various panel sections had thickness of 3.5 mm and 4.5 mm. Two different section properties were generated for the CRS, both incorporating the Belytschko-Tsay shell elements which were assigned thickness of 3.5 mm and 4.5 mm for both regions of the CRS. The material model *MAT_PIECEWISE_LINEAR_PLASTICITY, was used for the CRS polypropylene. Values for the density, Young's modulus, and Poisson's ratio were 800 kg/m^3, 0.842 GPa, and 0.3 respectively. As well a stress versus effective plastic strain curve obtained from the tensile testing results was assigned to the CRS material card. The mesh of the child seat was comprised of 12,728 nodes and 13,379 shell elements, among which 11935 elements were quadrilateral elements and 1444 elements were triangular elements. The final mesh of the deformable child safety seat is illustrated in Figure 5 and Figure 6.

(a) **(b)**

Figure 5. Front isometric view of the deformable CRS.

(a) **(b)**

Figure 6. Rear isometric view of the deformable CRS.

3.2 Modeling of the seatbelt restraints

The seatbelt was modeled to pass through a series of openings and channels of the CRS and to fit around the Hybrid III 3-year-old dummy, which had the same configuration as in all experimental tests. A portion of the seatbelt in the back of the CRS was modeled using one dimensional seatbelt elements, and was connected to the frontal part of the seatbelt which had contact with the child dummy by nodal rigid bodies.

The material model *MAT_FABRIC, was used for the seatbelt webbing. The density, Young's modulus, and Poisson's ratio were assigned to the seatbelt. Fully integrated Belytschko-Tsay membrane was used for the shell elements of the seatbelt. The webbing of the top tether and LATCH were modeled using one dimensional seatbelt elements. The material model *MAT_SEATBELT was used for the seatbelt elements. Loading and unloading curves obtained from the material testing were defined for the one dimensional seatbelt elements. *SECTION_SEATBELT was used to define the section properties of the seatbelt elements. Figure 7 illustrates the seatbelt, LATCH, top tether, and the five point restraint system.

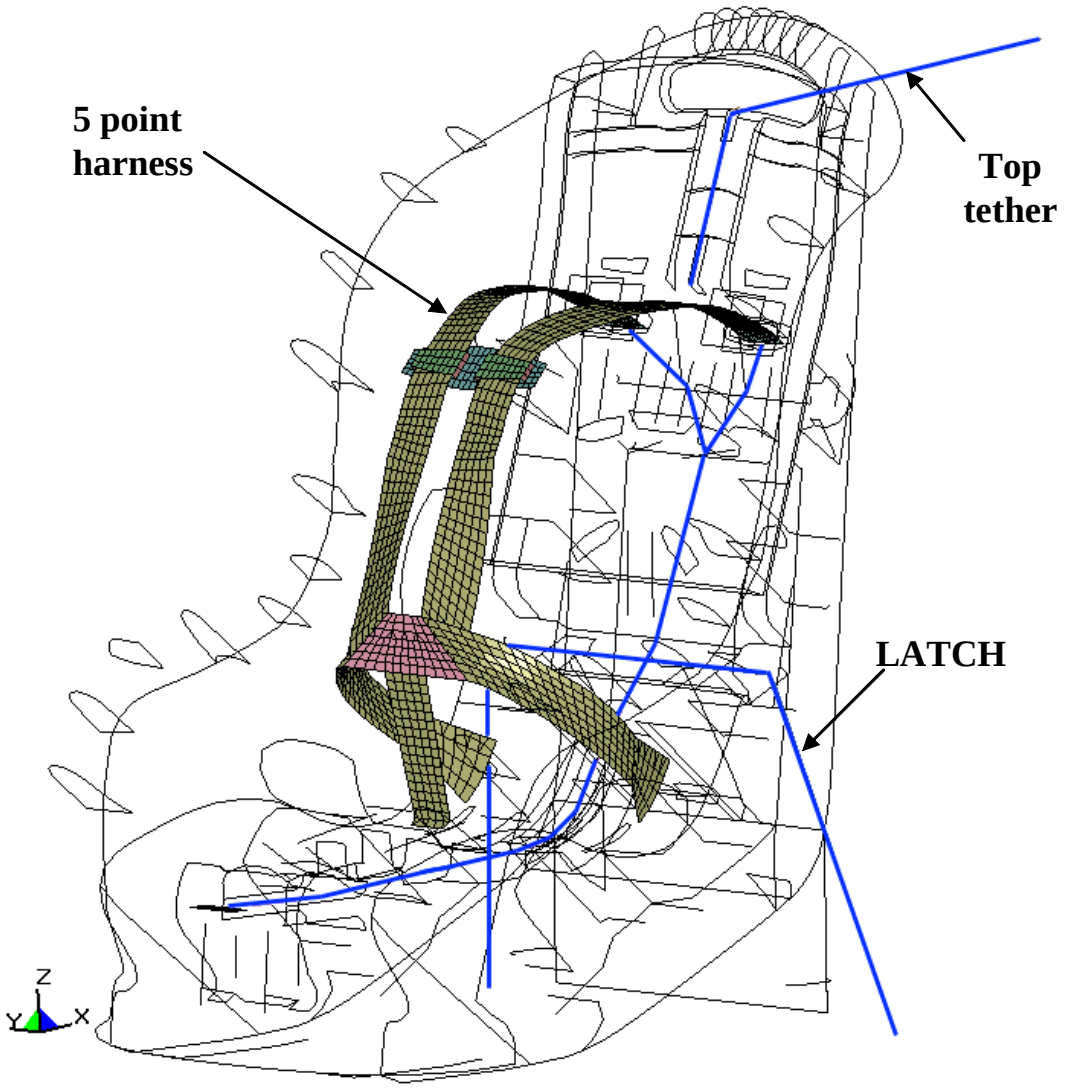

Figure 7. The seatbelt, LATCH, top tether, and the five point restraint system.

3.3 Modeling of the foam pad

A foam pad, which was inserted in between the polypropylene shell and the seat fabric of the CRS, was also incorporated into the FE model of the CRS. The foam was modeled using a selectively reduced solid element formulation. The material model *MAT_LOW_DENSITY_FOAM was used for solid elements. The mesh of the foam pad is shown in Figure 8.

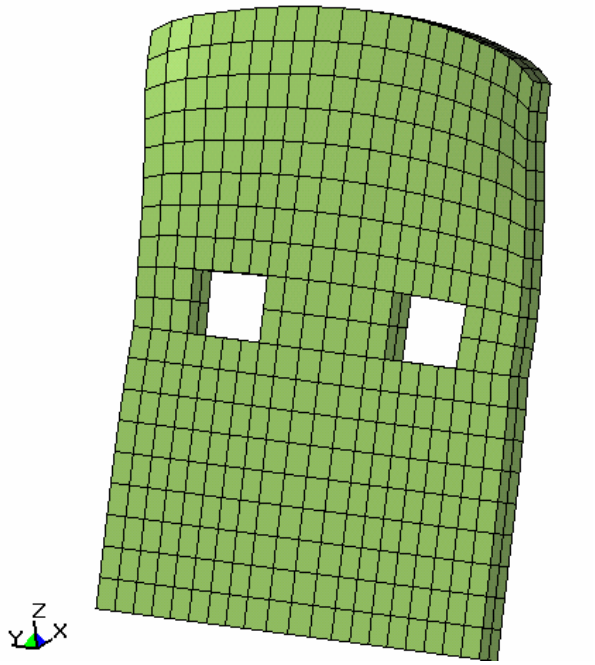

Figure 8. The mesh of the foam pad.

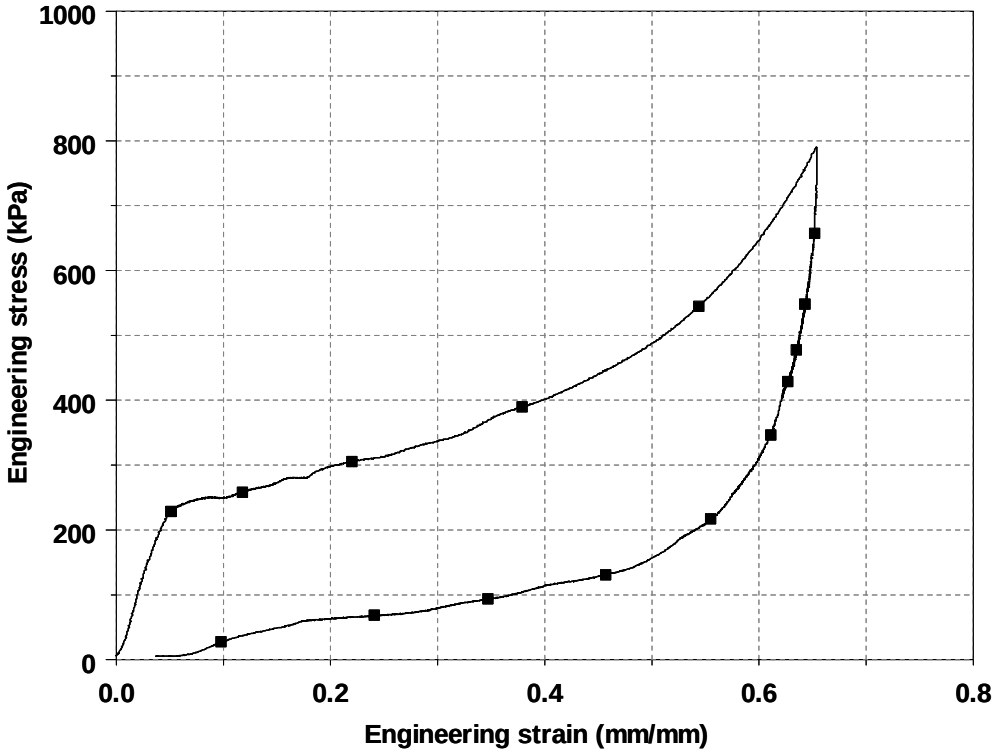

Figure 9. Engineering stress versus engineering strain response of the polymeric energy absorbing foam.

3.4 Modeling of the vehicle seat

Two parts were created in order to model the vehicle seat. The rigid car seat in the outside was modeled using shell elements, and the deformable car seat was modeled using solid elements. The two parts were connected using the keyword command *CONSTRAINED_EXTRA_NODES.

The numerical model of the Hybrid III three-year-old dummy (version 2.3-2) was provided by First Technology Safety Systems (FTSS). The complete FE model containing the child dummy, CRS, seat belt webbing, the waist and chest buckles, LATCH and the top tether, and the rigid and deformable vehicle seats is illustrated in Figure 10.

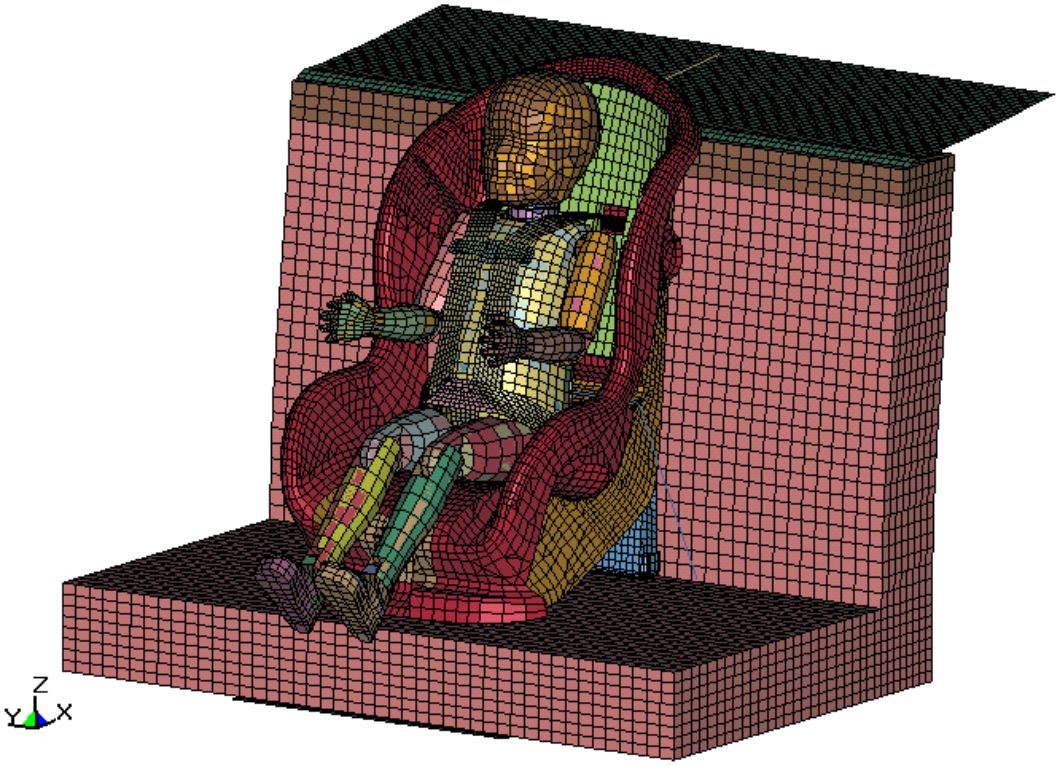

Figure 10. Complete FE model of the deformable CRS.

3.5 Basic setup of the simulation

Tightening of the front-adjusting harness strap was simulated to properly position the child dummy into the CRS from 0 to 40 ms. An acceleration pulse with the magnitude/time history as observed from the experimental tests was prescribed to the rigid car seat after tightening of the harness strap was completed. The ends of the top tether and LATCH were constrained to the rigid car seat using the keyword command *CONSTRAINED_EXTRA_NODES. A gravity force was applied to the whole system by using keyword *LOAD_BODY_Z.

Twenty-nine different contact algorithms were defined for modeling the contact between the child dummy and the CRS. All the computer simulations were conducted using LS-DYNA. The double precision version of LS-DYNA version 970 revision 5434a was used.

3.6 Suggested CRS modification for improved protection of children in side crashes

There are a considerable number of uncertainties in vehicle crash and child injury mechanisms for side impacts at the present time, which may inhibit the development of a novel device to significantly reduce the possibility of injury. In this research, the use of energy absorbing foams as a method to attenuate injuries in side impact has been investigated.

Modification to the original CRS was completed. Addition of a low density polymeric energy absorbing foam applied through the entire length of both side wings was considered. Figure 11 depicts the modified CRS with the additional side foam padding with uniform thickness of 20 mm. Material characteristics were identical to the padding on the back of the CRS. The foam was modeled using solid elements. The 1/2 sine - 90° side impact test was selected to investigate the injury attenuation possibilities with the application of the energy absorbing foam.

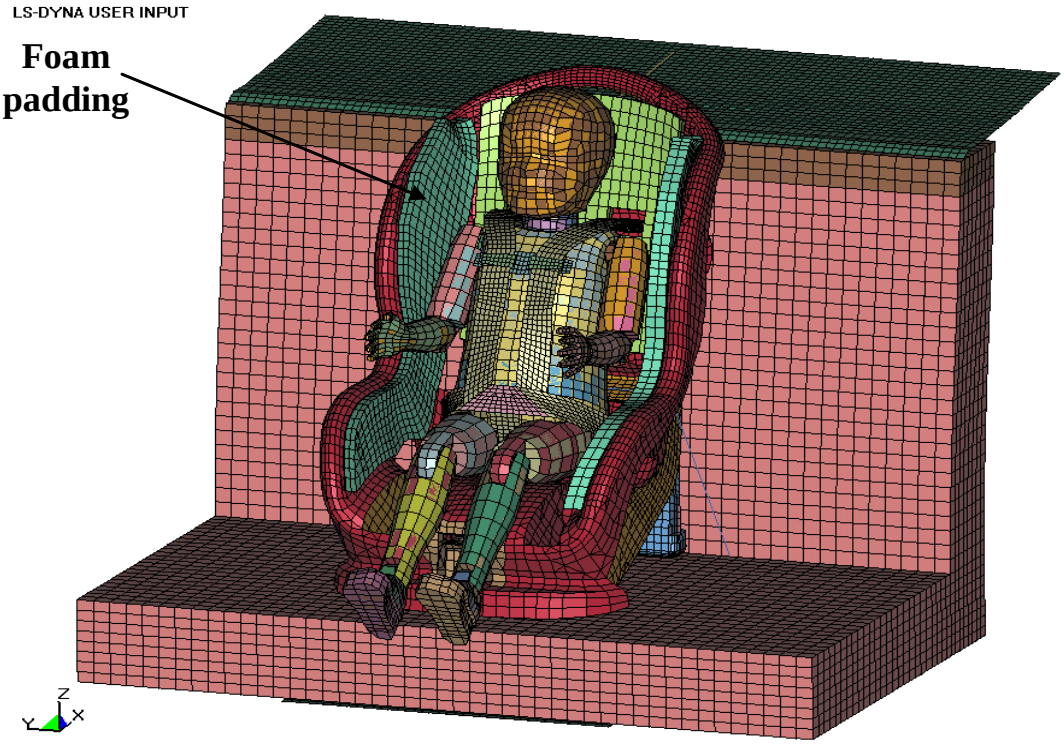

Figure 11. Child restraint seat model with foam padding.

Further studies were conducted to confine the lateral movement of the dummy's head by adding more energy absorbing foam in the region of the CRS where the child's head may come into contact with during side impacts. It was expected that during side crashes the dummy's head would immediately contact the energy absorbing foam and the deformation of the foam would help to reduce the injury parameters even further. Foam blocks were added on the previous foam padding. The nodes between the two volumes of foam were merged. The same material property and element formulation were assigned to the additional foam. The model with foam blocks in the head region of the CRS is shown in Figure 12.

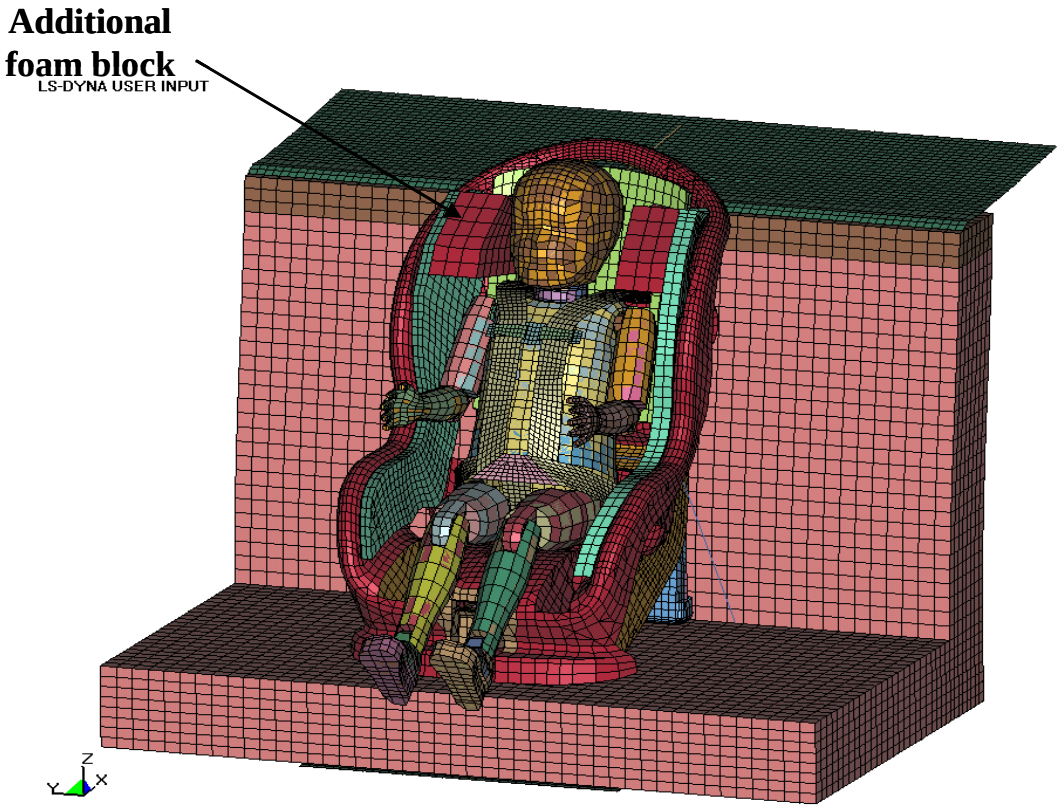

Figure 12. Child restraint seat model with foam blocks.

3.7 Data extraction of the Hybrid III 3-year-old child dummy model

Child occupant injury data were extracted from the two types of instrumentation that were found in the dummy model; accelerometers and load cells. Three nodes were defined as accelerometers, and nodal acceleration data were stored in the *nodout* American Standard Code for Information Interchange (ASCII) time history file. The output for the load cell beams was found in the *elout* ASCII time history file.

Due to the fact that human body parts respond to certain frequencies, standard SAE J211 [6] was utilized to filter all the experimental and numerical data. The filters for dummy data channels prescribed by SAE J211 are listed in Table 2.

Table 2. SAE J211 filters for child occupant injury data.

Injury data	Data channel
Head Acceleration	Class 1000
Neck Force	Class 1000
Neck Moment	Class 600
Chest Acceleration	Class 180

3.8 Head injury criteria

Equation 1 was used to determine the head injury criteria for the Hybrid III 3-year-old child dummy.

$$HIC = \left[\frac{1}{t_2 - t_1} \int_{t_1}^{t_2} a_{\text{resultant}} \cdot dt \right]^{2.5} \cdot (t_2 - t_1) \quad (1)$$

Where $$a_{\text{resultant}} = \sqrt{a_x{}^2 + a_y{}^2 + a_z{}^2} \quad (2)$$

4. Results and Discussions

Three side impact simulations were completed for data comparison. (i) using the half sine acceleration pulse with the seat oriented at 90° relative to the motion of the sled, (ii) using the half sine acceleration pulse with the seat oriented at 45° relative to the motion of the sled, and (iii) using a scaled FMVSS 213 acceleration pulse with the seat oriented at 90° relative to the motion of the sled. The accelerations versus time history were presented in Figures 4 and 5. A comparison of HIC values (calculated using a 15 ms, 36 ms, and unlimited time interval), chest accelerations, upper neck peak compression loads, and upper neck peak tension loads from the experimental and numerical tests are presented in Figure 13, Figure 14 and Figure 15.

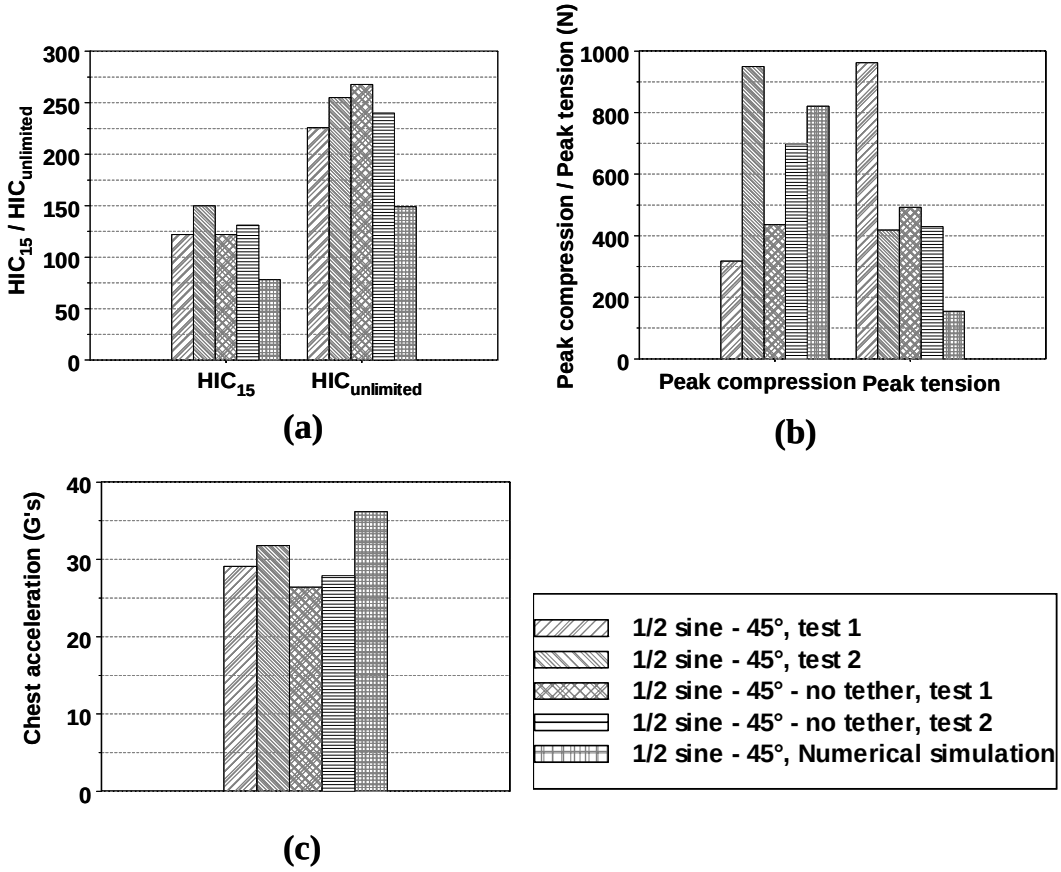

Figure 13. Experimental and numerical observations of (a) HIC values (b) upper neck compression and tension (c) chest accelerations from side impact tests (1/2 sine - 45°).

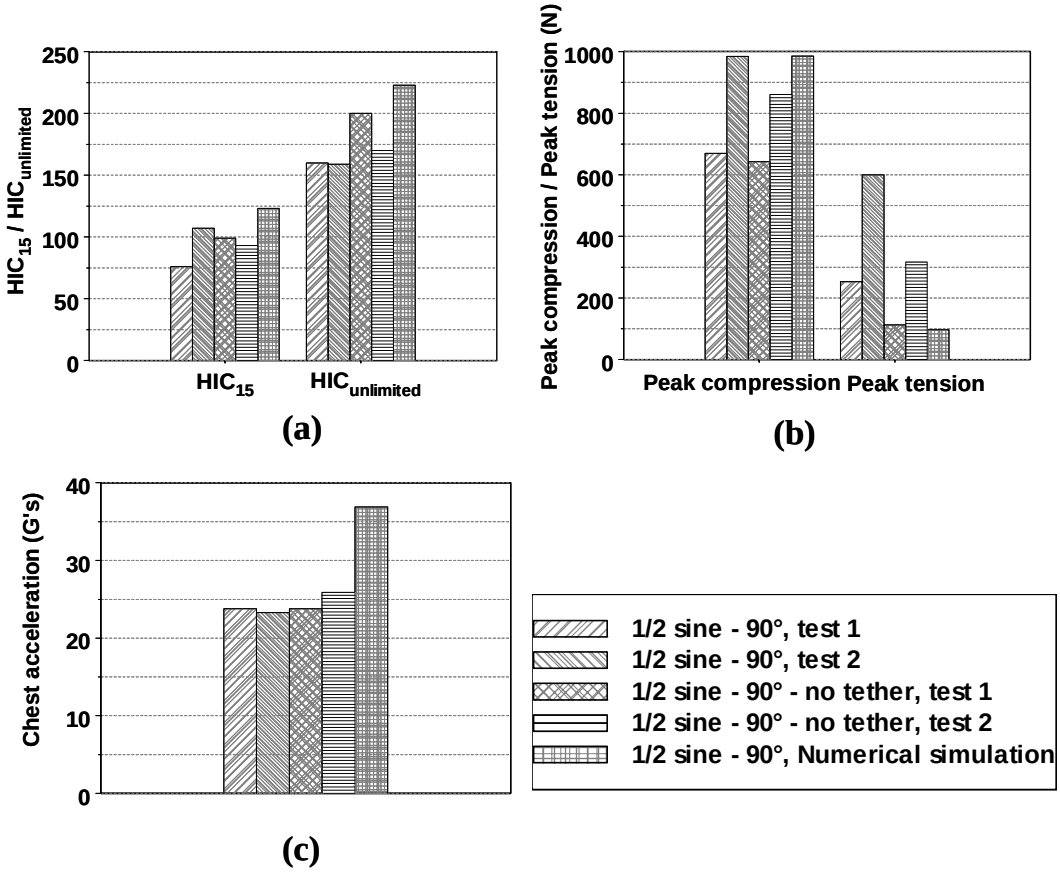

Figure 14. Experimental and numerical observations of (a) HIC values (b) upper neck compression and tension (c) chest accelerations from side impact tests (1/2 sine - 90°).

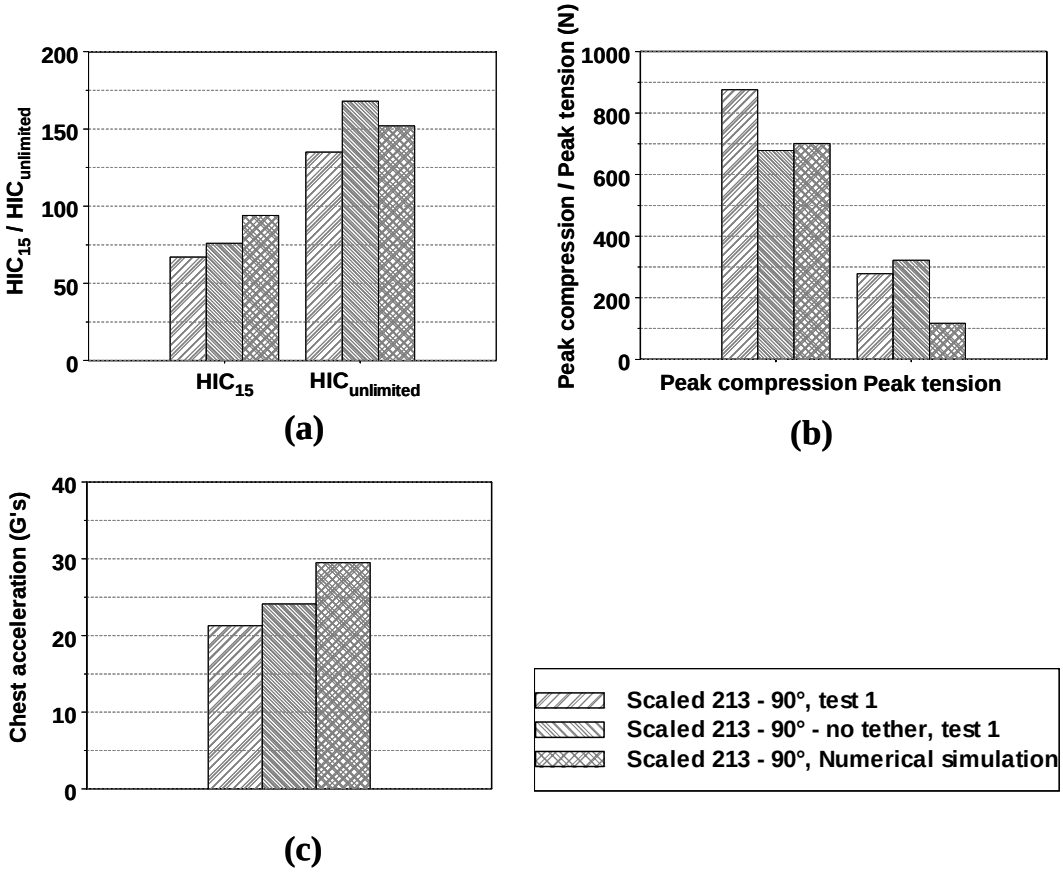

Figure 15. Experimental and numerical observations of (a) HIC values (b) upper neck compression and tension (c) chest accelerations from side impact tests (Scaled 213 - 90°).

An examination of Figures 13, 14, and 15 indicated that the results from the numerical simulations over predicted, under predicted, and fell in the upper and lower values of experimental testing results. However, a significant scatter in observations for all experimental tests was also evident. The discrepancies between the experimental and numerical data might be the results of different initial positions of the child dummy and different child restraints used. Specific details within the experimental tests such as child dummy positions were not completely revealed in FMVSS 213 ANPRM [5], thus it was difficult to use the exact same test configurations in the simulations.

Figure 16 (a) illustrates the numerical kinematic observations from this research and Figure 16 (b) illustrates experimental observations of a side impact test completed in a similar condition [7] to the numerical simulation. Both tests were considered far side impact tests, in which seating position was on the opposite side from the point of impact. Overall, the kinematic responses of the child dummies and the child restraints in both the experimental and numerical side impact tests were comparable.

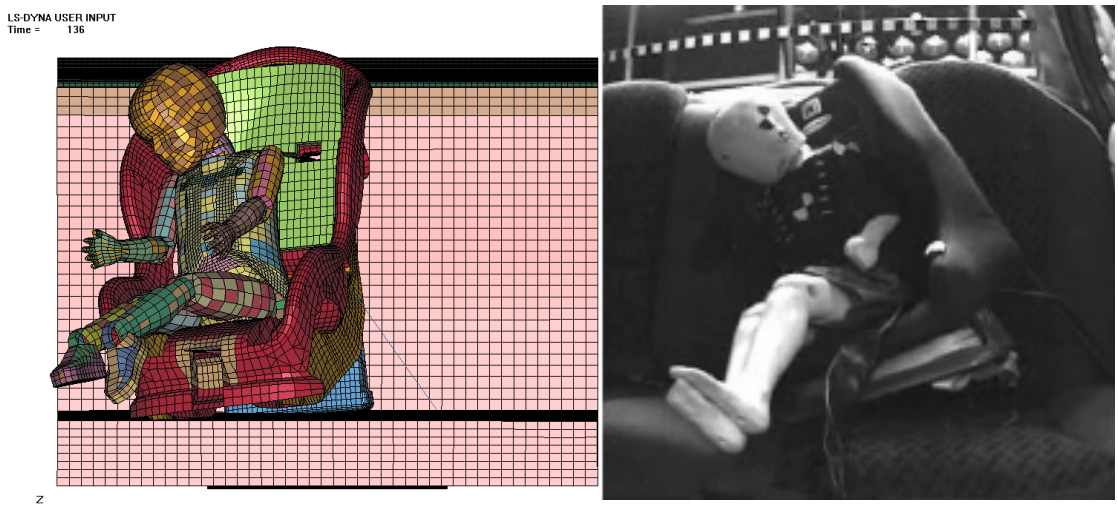

(a) **(b)**

Figure 16. (a) Numerical and (b) experimental [7] observations of side impact tests.

Numerical simulations incorporating countermeasure for side impacts were completed and a summary of *HIC* values and chest accelerations is shown in Table 3.

Table 3. Numerical comparisons of side impact tests with and without the foam padding.

Numerical Simulations	Injury Parameters		
	HIC_{15}	HIC_{36}	Chest Accel. (G's)
1/2 sine - 90°	123	216	36.9
1/2 sine - 90° with foam	74	136	29.5

It was observed that HIC values decreased approximately 40 percent and chest accelerations decreased approximately 20 percent when the child dummy was protected with energy absorbing foam during side impacts. These results suggest that foam padding may be very effective in reducing the injury potential of the children in side impacts.

A parametric study was conducted to investigate the effect of foam stress versus strain response on the injury risk of the child dummy. A simulation was completed with an unaltered stress versus strain response for the polymeric foam. Two further simulations with the stress scaled by factors of two and five were completed. The results of HIC values and chest accelerations are summarized in Table 4.

Table 4. Parametric study of the effects of foam stiffness on the injury potential of the child dummy.

Numerical Simulations	Injury Parameters		
	HIC_{15}	HIC_{36}	Chest Accel. (G's)
Without foam padding	123	216	36.9
Foam padding	74	136	29.5
Foam padding + foam blocks (scale factor = 1)	74	130	36.2
Foam padding + foam blocks (scale factor = 2)	76	139	38.5
Foam padding + foam blocks (scale factor = 5)	91	123	35.9

Data in the table showed that adding extra foam blocks did not necessarily reduce the likelihood of injury for the children positioned in the far side configuration. The HIC values and chest accelerations remained at approximately the same level. Illustration of the kinematic response as presented in Figure 17 showed that although the use of a stiffer foam block resulted in less lateral displacement of the dummy's head, the overall kinematic responses of the dummies were very similar to the one without foam blocks. These testing conditions were only applicable to far side crashes. It is expected that for near side crash conditions the improvement in any parameters might be much more significant due to contact between the vehicle interior and the CRS. The deformation of the foam blocks would prevent the head from direct contact with the vehicle door and as a result, the child might have a better chance to survive in a near side crash condition.

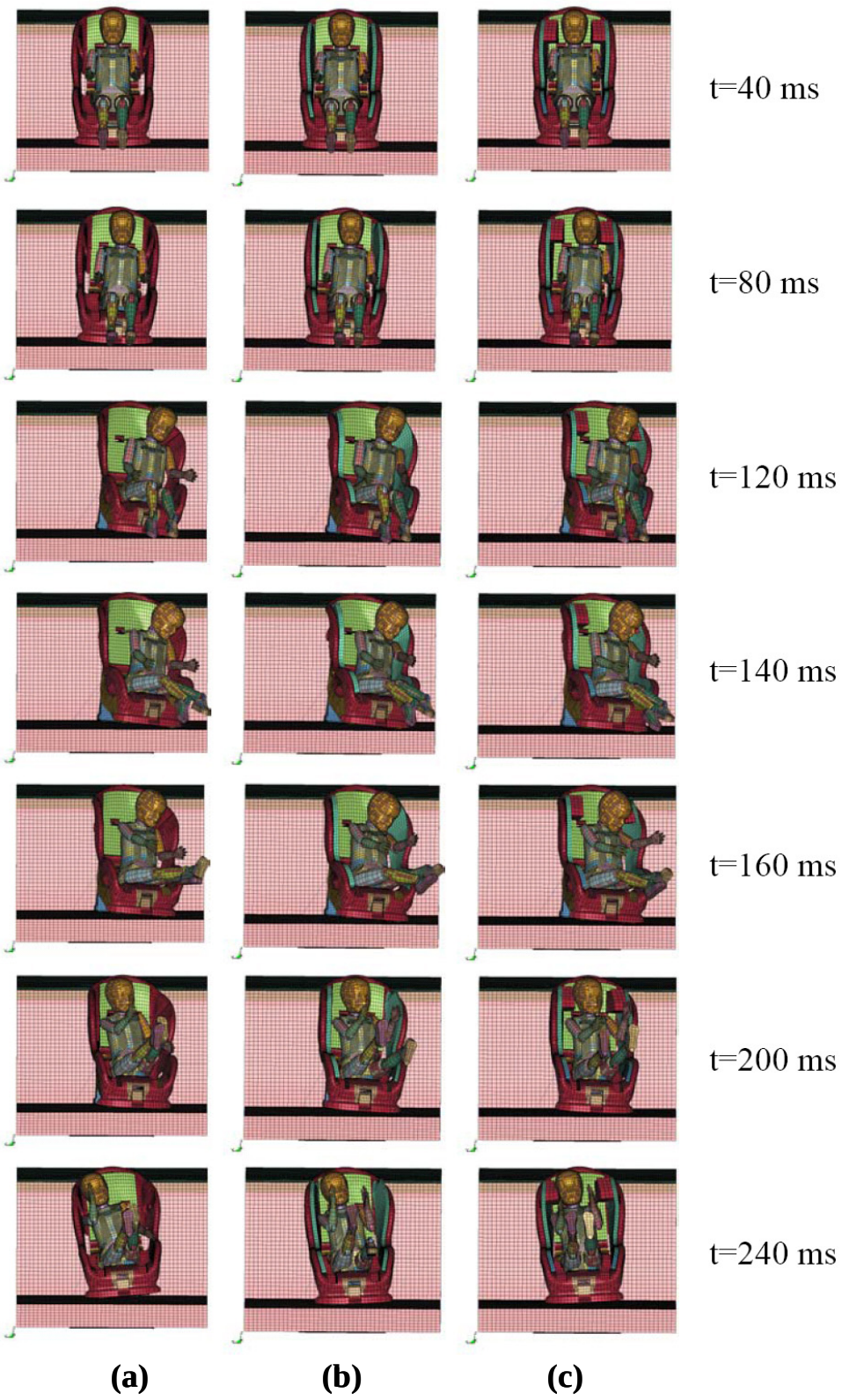

Figure 17. Kinematic responses of the child dummies (a) without foam padding (b) with foam padding (c) with foam padding and foam blocks.

5. Conclusions

1. The deformable model was used to investigate the injury potential of the Hybrid III 3-year-old child dummy in side impact crashes.

2. Side impact data comparisons were conducted between the simulation results from the complex model and experimental findings in standard FMVSS 213 ANPRM [5]. It was observed that for the numerical simulations head injury criteria values, chest accelerations, and upper neck peak compression and peak tension were normally close to the experimental test data.

3. The use of energy absorbing foams as a method to attenuate injuries in side impact has been investigated. It was observed from the simulation results that foam padding was effective in reducing the head and chest injury potential of the child dummy in side crashes by approximately 40 and 20 percent respectively.

4. Further studies were conducted to confine lateral movement of the dummy's head by adding more energy absorbing foam blocks in the head region of the CRS. It was observed that with the extra foam blocks HIC values and chest accelerations remained at approximately the same level.

Reference

1. Traffic Safety Facts 2004, DOT HS 809 607, U.S. Department of Transportation, National Highway Traffic Safety Administration, pp. 1-6, 2004.

2. Final rule, Federal Motor Vehicle Safety Standards 213; Child Restraint Systems, 49 CFR Part 571, Docket No. NHTSA–03–15351, *Federal Register*, Vol. 68, No. 121, pp. 1-40, Tuesday, June 24, 2003.

3. A. Howard, L. Rothman, A. Moses, J. Pazmino-Canizares, B. Monk, J. Comeau, D. Mills, S. Beng, I. Hale, and A. German, Children in Side-Impact Motor Vehicle Crashes: Seating Positions and Injury Mechanisms, *The Journal of TRAUMA Injury, Infection, and Critical Care*, Vol. 56, pp. 1276 –1285, 2004.

4. A. Howard, Child safety in frontal and side impacts, Presentation at Ford Motor Company, Hospital for Sick Kids, May 2005.

5. Advance notice of proposed rulemaking (ANPRM), Federal Motor Vehicle Safety Standards 213; Child Restraint Systems, 49 CFR Part 571, Docket No. 02–12151, *Federal Register*, Vol. 67, No. 84, pp. 1-17, Wednesday, May 1, 2002.

6. SAE J211/1 Instrumentation for Impact Test - Part 1– Electronic Instrumentation, *Society of Automotive Engineers*, Warrendale PA., 2003.

7. J. Charlton, B. Fildes, R. Laemmle, S. Smith, and F. Douglas, A Preliminary Evaluation of Child Restraint Crash Performance with Three Anchorage Systems in a Holden Commodore, http://www.rsconference.com/pdf/RS040079.pdf, pp. 1-10, Accessed Jan 2006.